PROCEEDINGS OF SCIENCE

Scale-Invariant Model for Gravitational Waves and Dark Matter

Alexandros Karam*
Laboratory of High Energy and Computational Physics,
National Institute of Chemical Physics and Biophysics, Rävala pst. 10, 10143 Tallinn, Estonia;
E-mail: alexandros.karam@kbfi.ee

Maciej Kierkla and Bogumiła Świeżewska
Faculty of Physics, University of Warsaw, Pasteura 5, 02-093 Warsaw, Poland;
E-mail: maciej.kierkla@fuw.edu.pl; bogumila.swiezewska@fuw.edu.pl

The present contribution summarises the results recently published in Ref. [1]. We have conducted a revised analysis of the first-order phase transition that is associated with symmetry breaking in a classically scale-invariant model that has been extended with a new $SU(2)$ gauge group. By incorporating recent developments in the understanding of supercooled phase transitions, we were able to calculate all of its features and significantly limit the parameter space. We were also able to predict the gravitational wave spectra generated during this phase transition and found that this model is well-testable with LISA. Additionally, we have made predictions regarding the relic dark matter abundance. Our predictions are consistent with observations but only within a narrow part of the parameter space. We have placed significant constraints on the supercool dark matter scenario by improving the description of percolation and reheating after the phase transition, as well as including the running of couplings. Finally, we have also analyzed the renormalization-scale dependence of our results.

Corfu Summer Institute 2022 "School and Workshops on Elementary Particle Physics and Gravity",
28 August - 1 October 2022,
Corfu, Greece

*Speaker.

PoS(CORFU2022)106

1. Introduction

Considering the recent direct detection of gravitational waves (GW) by the LIGO and Virgo Collaborations [2–7], as well as the upcoming Laser Interferometer Space Antenna (LISA) [8–13] and other future and ongoing experiments [14–23], it is reasonable to explore ways to utilize GW to investigate fundamental physics. One promising method is to search for evidence of a first-order phase transition (PT) in the early Universe through the primordial gravitational wave background [9–13,24]. This signal is expected to be present at frequencies within LISA's sensitivity range if the transition occurred around temperatures similar to those of the electroweak PT, $T \sim 100$ GeV. However, in many models, the signal is not strong enough to be detected. In contrast, the class of models with classical scale invariance [25–38] typically predicts a strong gravitational wave signal within LISA's reach due to a logarithmic potential that enables significant supercooling and latent heat release during the transition.

Within the wide variety of classically conformal models, those incorporating an additional gauge group are particularly promising due to their high level of predictability. The conformal Standard Model (SM) can be extended in a minimal manner with the addition of either an extra $U(1)$ [28, 33, 34, 36–70] or $SU(2)$ [25, 31, 32, 50, 64, 71–76] symmetry, and there are other possibilities such as models featuring an extended scalar sector [29, 30, 40, 50, 77–118], larger gauge groups, extra fermions, or more intricate architectures [119–138]. The focus of our current work is on the first-order PT in a classically scale-invariant model that includes an additional $SU(2)_X$ gauge symmetry and a scalar that transforms as a doublet under this group while remaining a singlet of the SM. In addition to exhibiting a strong first-order phase transition, this model also provides a candidate for dark matter particles that are stabilized by a residual symmetry that persists after the $SU(2)_X$ symmetry is broken [139, 140].

Although the possibility of detecting GW from a PT and exploring events that occurred in the early Universe is exciting, the imprecise nature of theoretical predictions is discouraging [141,142]. The dependence on the renormalisation scale is one of the main sources of uncertainty in these predictions. Classically scale-invariant models, owing to the logarithmic nature of their potential, span a broad range of energies and therefore are particularly susceptible to issues related to scale dependence. In this work [1]:

1. We present updated predictions of the stochastic GW background in the classically scale-invariant model with $SU(2)_X$ symmetry, incorporating recent advances in understanding supercooled PTs [143–147]. Our study is the first to include the condition for percolation in the SU$(2)_X$ model, and we show that it significantly affects the parameter space.

2. We pay close attention to the renormalisation-scale dependence of the results. To minimise this dependence, we use a renormalisation-group improved effective potential and perform an expansion in powers of couplings consistent with the conditions from conformal symmetry breaking and the radiative nature of the transition.

3. We investigate the DM phenomenology in light of the updated understanding of the PT.

2. The model

In this work [1], we analyse the classically scale-invariant SM extended by a dark $SU(2)_X$ gauge group. The new fields of the model are:

- the scalar doublet Φ of $SU(2)_X$,
- the three dark gauge bosons X of $SU(2)_X$.

The Higgs H and new scalar Φ doublets can be written as

$$H = \frac{1}{\sqrt{2}} \begin{pmatrix} 0 \\ h \end{pmatrix}, \quad \Phi = \frac{1}{\sqrt{2}} \begin{pmatrix} 0 \\ \varphi \end{pmatrix}.$$

In terms of h and φ, the one-loop effective potential can be written as

$$V(h,\varphi) = V^{(0)}(h,\varphi) + V^{(1)}(h,\varphi), \tag{2.1}$$

where the tree-level part is

$$V^{(0)}(h,\varphi) = \frac{1}{4}\left(\lambda_1 h^4 + \lambda_2 h^2 \varphi^2 + \lambda_3 \varphi^4\right), \tag{2.2}$$

with λ_2 being the portal coupling that connects the visible and dark sectors. The one-loop correction is given by

$$V^{(1)}(h,\varphi) = \frac{1}{64\pi^2} \sum_a n_a M_a^4(h,\varphi) \left(\log \frac{M_a^2(h,\varphi)}{\mu^2} - C_a\right), \tag{2.3}$$

where

$$n_a = (-1)^{2s_a} Q_a N_a (2s_a + 1),$$

and the sum runs over all particle species. With $M_a(h,\varphi)$ we denote the field-dependent mass of a particle, n_a denotes the number of degrees of freedom associated with each species and $C_a = \frac{5}{6}$ for vector bosons and $C_a = \frac{3}{2}$ for other particles. Furthermore, $Q_a = 1$ for uncharged particles, and $Q_a = 2$ for charged particles, $N_a = 1, 3$ for uncoloured and coloured particles, respectively.

Regarding symmetry breaking, the stationary point equations divided by the VEVs, $v = \langle h \rangle$, $w = \langle \varphi \rangle$, read

$$\frac{1}{v^3}\frac{\partial V}{\partial h} = \lambda_1 + \frac{1}{2}\lambda_2 \left(\frac{w}{v}\right)^2 + \frac{1}{v^3}\left.\frac{\partial V^{(1)}}{\partial h}\right|_{h=v,\varphi=w} = 0, \tag{2.4}$$

$$\frac{1}{w^3}\frac{\partial V}{\partial \varphi} = \lambda_3 + \frac{1}{2}\lambda_2 \left(\frac{v}{w}\right)^2 + \frac{1}{w^3}\left.\frac{\partial V^{(1)}}{\partial \varphi}\right|_{h=v,\varphi=w} = 0. \tag{2.5}$$

Typically, $v_\varphi/v_h \gg 10$, therefore the $\lambda_2 \left(v_h/v_\varphi\right)^2$ term can be neglected. Then, the second equation becomes

$$\lambda_3 = -\frac{9}{256\pi^2} g_X^4 \left[2\log\left(\frac{g_X}{2}\frac{w}{\mu}\right) - \frac{1}{3}\right]. \tag{2.6}$$

The first equation reads

$$\lambda_1 + \frac{1}{2}\lambda_2\left(\frac{w}{v}\right)^2 + \frac{1}{16\pi^2}\sum_{W^\pm,Z,t} n_a \frac{M_a^4(h,\varphi)}{v^4}\left(\log\frac{M_a^2(h,\varphi)}{\mu^2} - C_a + \frac{1}{2}\right) = 0. \tag{2.7}$$

The above indicates that the symmetry breaking in the φ direction follows the Coleman-Weinberg mechanism, while the symmetry breaking in the direction of h is similar to that of the SM, as the "tree-level mass term" is generated by the portal coupling.

The physical mass corresponds to a pole of the propagator, i.e. is evaluated away from $p^2 = 0$, and is given by

$$M^2_{\text{pole}} = m^2_{\text{tree-level}} + \text{Re}[\Sigma(p^2 = M^2_{\text{pole}})]. \tag{2.8}$$

Including loop corrections from self energies which introduce momentum dependence, we have

$$M^2(p) = \begin{pmatrix} 3\lambda_1 v^2 + \frac{\lambda_2}{2} w^2 & \lambda_2 v w \\ \lambda_2 v w & 3\lambda_3 w^2 + \frac{\lambda_2}{2} v^2 \end{pmatrix} + \begin{pmatrix} \Sigma_{hh}(p) & \Sigma_{h\varphi}(p) \\ \Sigma_{h\varphi}(p) & \Sigma_{\varphi\varphi}(p) \end{pmatrix}. \tag{2.9}$$

By diagonalising the mass matrix we obtain the mass eigenvalues

$$\begin{aligned} M^2_\pm(p^2) = \frac{1}{2}\Bigg\{ &\left(3\lambda_1 + \frac{\lambda_2}{2}\right)v^2 + \frac{1}{2}\left(\frac{\lambda_2}{2} + 3\lambda_3\right)w^2 + \Sigma_{hh}(p^2) + \Sigma_{\varphi\varphi}(p^2) \\ &\pm \sqrt{\left[\left(3\lambda_1 - \frac{\lambda_2}{2}\right)v^2 - \left(3\lambda_3 - \frac{\lambda_2}{2}\right)w^2 + \Sigma_{hh}(p^2) - \Sigma_{\varphi\varphi}(p^2)\right]^2 + 4\lambda_2^2 v^2 w^2}\Bigg\}. \end{aligned} \tag{2.10}$$

Neglecting terms suppressed by a product of a small coupling, λ_2 or λ_3 and the Higgs VEV, we can approximately determine which of the mass eigenvalues corresponds to the Higgs particle. We find

$$M^2_+(h,\varphi) = 3\lambda_3\varphi^2 + \Sigma_{\varphi\varphi}(p^2), \tag{2.11}$$

$$M^2_-(h,\varphi) = 3\lambda_1 h^2 + \frac{1}{2}\lambda_2\varphi^2 + \Sigma_{hh}(p^2). \tag{2.12}$$

for $3\lambda_1 h^2 - 3\lambda_3\varphi^2 + \frac{1}{2}\lambda_2\varphi^2 + \Sigma_{hh}(p^2) - \Sigma_{\varphi\varphi}(p^2) < 0$. For the opposite sign, M_+ and M_- are interchanged. Then, to obtain the momentum-corrected masses we solve the gap equations

$$M_H^2 = M^2_\mp(p^2 = M_H^2), \tag{2.13}$$

$$M_S^2 = M^2_\pm(p^2 = M_S^2). \tag{2.14}$$

We identify the first one with the Higgs $M_H = 125\,\text{GeV}$, while the other gives the mass of the new scalar S. Finally, the mass eigenstates are obtained from the gauge eigenstates by a rotation matrix as

$$\begin{pmatrix} \phi_- \\ \phi_+ \end{pmatrix} = \begin{pmatrix} \cos\theta & \sin\theta \\ -\sin\theta & \cos\theta \end{pmatrix}\begin{pmatrix} h \\ \varphi \end{pmatrix}, \qquad -\frac{\pi}{2} < \theta < \frac{\pi}{2}. \tag{2.15}$$

In order to scan the parameter space, we employ the following numerical procedure:

1. We choose the values of the input parameters, M_X and g_X. We assume the tree-level relation for the X mass $M_X = \frac{1}{2} g_X v_\varphi$ so we can compute the value of the φ VEV, v_φ. The values of g_X and v_φ are treated as evaluated at the scale $\mu = M_X$.

2. We use the minimisation condition along the φ direction, evaluated at $\mu = M_X$ to evaluate λ_3. This gives us a simple relation

$$\lambda_3 = \frac{3}{256\pi^2} g_X^4.$$

3. The g_X and λ_3 couplings are evolved using their RGEs and evaluated at $\mu = M_Z$.

4. If $g_X(M_Z) \leqslant 1.15$ the RG-improved potential is well-behaved throughout the scales considered.

5. The value of λ_2 as a function of $\lambda_1(\mu = M_Z)$ is obtained from the first minimisation condition.

6. The value of λ_1 is computed from the requirement that the physical Higgs mass is equal to 125 GeV, using the first gap equation. The evaluation is performed at $\mu = M_Z$, therefore the vacuum expectation value of φ at $\mu = M_Z$ is needed. It is found using the second minimisation condition evaluated at $\mu = M_Z$.

7. The mass of S is computed by solving iteratively the second gap equation.

8. The mixing between the scalars is evaluated by demanding that the off-diagonal terms of the mass matrix evaluated at $p^2 = 0$ and in the mass-eigenbasis are zero.

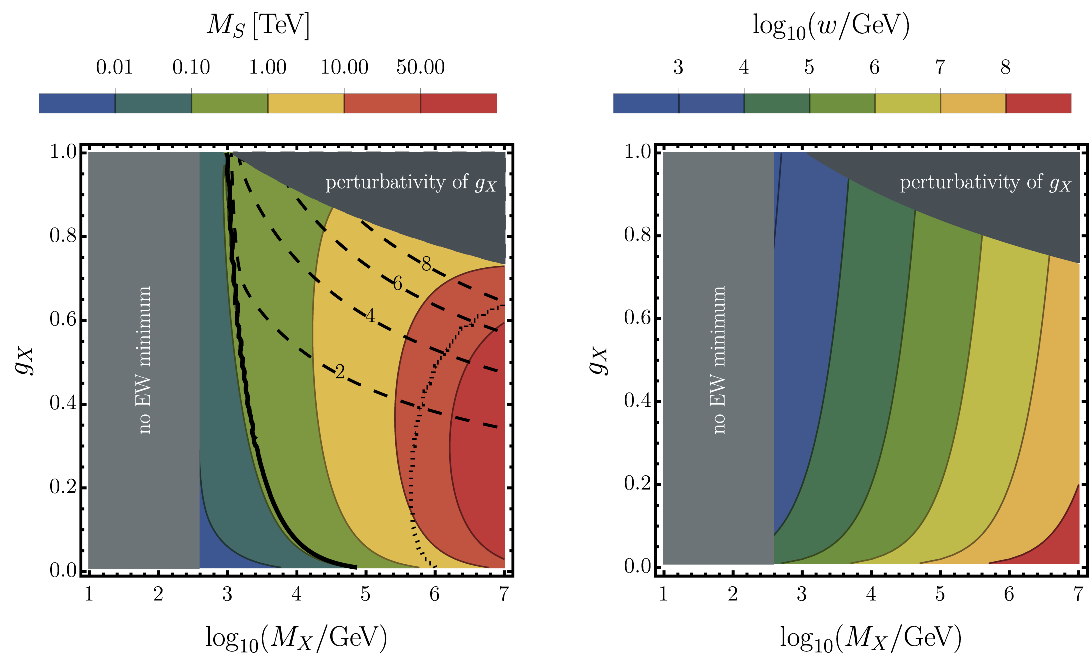

Figure 1: Values of the new scalar mass M_S (left panel) and the VEV w (evaluated at $\mu = M_X$) (right panel). In the left panel the thick black line indicates where $M_S = M_H = 125\,\text{GeV}$ and across this line mass ordering between S and H changes (to the left of the line $M_S < M_H$, and to the right $M_H < M_S$). To the right of the dotted line ξ_H becomes numerically equal to 1. The dashed lines indicate a discrepancy between the running and the pole mass (in percent). Grey-shaded regions are excluded.

We present the result of the scan for M_S and w (the VEV of φ) in figure 1. The new scalar S is heavier than the Higgs boson in most of the parameter space. The dashed lines in the plot represent the disparity between the mass obtained by solving eq. (2.14) iteratively and the mass estimated from the effective potential approximation. Although the differences are not negligible, they do not exceed 10% even in the upper right region of the parameter space. Finally, the region of low X masses is excluded because it is not possible the reproduce a stable minimum with the correct Higgs VEV and mass in this regime, while the upper right corner is cut off by the condition $g_X(M_Z) \leq 1.15$ for the perturbativity of the dark gauge coupling.

3. Dark matter

Our DM candidates are the three vector bosons X^a_μ (where $a = 1, 2, 3$) of the hidden sector gauge group $SU(2)$ with mass $M_X = \frac{1}{2} g_X w$. As discussed in [139], the gauge bosons are stable due to an intrinsic $\mathbb{Z}_2 \times \mathbb{Z}_2'$ symmetry associated with complex conjugation of the group elements and discrete gauge transformations. This discrete symmetry actually generalizes to a custodial $SO(3)$ [140] and the dark gauge bosons are degenerate in mass.

For the standard freeze-out mechanism, the Boltzmann equation has the form

$$\frac{\mathrm{d}n}{\mathrm{d}t} + 3Hn = -\frac{\langle\sigma v\rangle_{\mathrm{ann}}}{3}\left(n^2 - n_{eq}^2\right) - \frac{2\langle\sigma v\rangle_{\mathrm{semi}}}{3} n\left(n - n_{eq}\right) . \tag{3.1}$$

The annihilation cross section is dominated by the $XX \to SS$ process

$$\langle\sigma v\rangle_{\mathrm{ann}} = \frac{11 g_X^4}{2304\pi M_X^2} , \tag{3.2}$$

while the semiannihilation cross section is dominated by the $XX \to XS$ process

$$\langle\sigma v\rangle_{\mathrm{semi}} = \frac{3 g_X^4}{128\pi M_X^2} . \tag{3.3}$$

Interestingly, the semiannihilation processes dominate since $\langle\sigma v\rangle_{\mathrm{semi}} \sim 5\langle\sigma v\rangle_{\mathrm{ann}}$.

Solving the Boltzmann equation, we obtain the dark matter relic abundance

$$\Omega_X h^2 = \frac{1.04 \times 10^9\ \mathrm{GeV}^{-1}}{\sqrt{g_*} M_P J(x_f)}, \qquad J(x_f) = \int_{x_f}^{\infty} dx \frac{\langle\sigma v\rangle_{\mathrm{ann}} + 2\langle\sigma v\rangle_{\mathrm{semi}}}{x^2} , \tag{3.4}$$

where $x_f \approx 25 - 26$ and $x = M_X/T$. The correct relic abundance $\Omega_{\mathrm{DM}} h^2 = 0.120 \pm 0.001$ is reproduced if

$$g_X \approx 0.9 \times \sqrt{\frac{M_X}{1\ \mathrm{TeV}}} . \tag{3.5}$$

Finally, DM particles can scatter off of nucleons, with the spin-independent cross section given by

$$\sigma_{\mathrm{SI}} = \frac{m_N^4 f^2}{16\pi v^2}\left(\frac{1}{M_S^2} - \frac{1}{M_H^2}\right)^2 g_X^2 \sin^2 2\alpha \simeq \frac{64\pi^3 f^2 m_N^4}{81 M_X^6} \approx 0.6 \times 10^{-45}\ \mathrm{cm}^2 \left(\frac{\mathrm{TeV}}{\mathrm{M_X}}\right)^6 . \tag{3.6}$$

Then, to evade the experimental bounds we would have $\sigma_{\mathrm{SI}} < 1.5 \times 10^{-45}\ \mathrm{cm}^2\ (\mathrm{M_X/TeV})$ for $M_X > 0.88\,\mathrm{TeV}$.

4. Finite temperature

The temperature-dependent effective potential is

$$V(h,\varphi,T) = V^{(0)}(h,\varphi) + V^{(1)}(h,\varphi) + V^{T}(h,\varphi,T) + V_{\rm daisy}(h,\varphi,T). \tag{4.1}$$

The finite-temperature correction is

$$V^{T}(h,\varphi,T) = \frac{T^4}{2\pi^2}\sum_a n_a J_a\left(\frac{M_a(h,\varphi)^2}{T^2}\right), \tag{4.2}$$

where the sum runs over particle species. J_a denotes the thermal function, which is given by

$$J_{F,B}(y^2) = \int_0^\infty \mathrm{d}x\, x^2 \log\left(1 \pm e^{-\sqrt{x^2+y^2}}\right), \tag{4.3}$$

where "+" for fermions (J_F) and "−" for bosons (J_B). The correction from the daisy-resummed diagrams is

$$V_{\rm daisy}(h,\varphi,T) = -\frac{T}{12\pi}\sum_i n_i\left[(M^2_{i,\rm th}(h,\varphi,T))^{3/2} - (M_i^2(h,\varphi))^{3/2}\right], \tag{4.4}$$

where n_i is the number of degrees of freedom, $M_{i,\rm th}$ denotes thermally corrected mass, and M_i the usual field dependent mass.

The zero-temperature part of the effective potential along the φ direction reads

$$V(\varphi) = \frac{1}{4}\lambda_3(t)Z_\varphi(t)^2\varphi^4 + \frac{9M_X(\varphi,t)^4}{64\pi^2}\left(\log\frac{M_X(\varphi,t)^2}{\mu^2} - \frac{5}{6}\right), \tag{4.5}$$

where $t = \log\frac{\mu}{\mu_0}$, $\mu_0 = M_Z$, $M_X(\varphi,t) = \frac{1}{2}g_X(t)\sqrt{Z_\varphi(t)}\varphi$, $\mu = \frac{1}{2}g_X(M_X)\varphi \equiv \overline{M}_X(\varphi)$.

Note that we include more terms in the renormalisation-group improved potential than in the approaches often found in the literature. In detail:

1. The approach of [31,64] approximates the running quartic coupling via its β function, relates the renormalisation scale with the field and uses as a reference scale the scale at which λ_φ changes sign,
$$V_1 \approx \frac{1}{4}\lambda_3(t)\varphi^4 \approx \frac{1}{4}\frac{9g_X^4}{128\pi^2}\log\left(\frac{\varphi}{\varphi_0}\right), \tag{4.6}$$
where $t = \log\frac{\mu}{\varphi_0}$, $\lambda_\varphi(0) = 0$ and g_X is evaluated at $\mu = \varphi_0$ (the running of g_X is not included).

2. The approach of [147] also approximates the one-loop potential by the tree-level potential with running coupling but uses $\mu = \varphi$ and some fixed reference scale $\mu_0 = m_t$,
$$V_2 \approx \frac{1}{4}\lambda_3(t)\varphi^4, \tag{4.7}$$
where $t = \log\left(\frac{\varphi}{\mu_0}\right)$.

To better understand which contributions are crucial we perform a series of approximations or modifications on our approach, the results of which are presented in the right panel of figure 2. Namely:

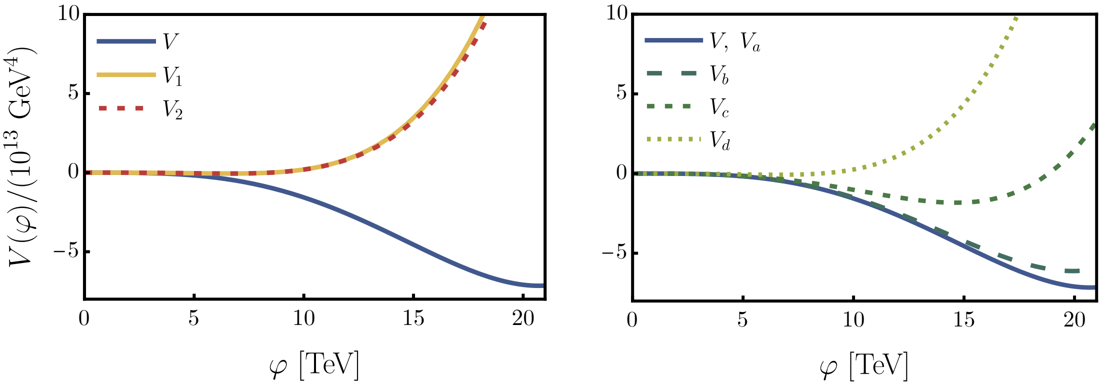

Figure 2: Effective potential at zero temperature along the φ direction for a benchmark point with $g_X = 0.9$, $M_X = 10^4$ GeV (defined at $\mu = M_X$). Left panel: Comparison of different approaches used in the literature, V_1 of eq. (4.6) (yellow solid), V_2 of eq. (4.7) (dashed red) and the full potential V of eq. (4.5) used in this work (solid blue). Right panel: Comparison of different approximations imposed on the full potential V of eq. (4.5) used in this work (solid blue) discussed in the main text: V_b (long-dashed darkest green), V_c (medium-dashed dark green), V_d (short-dashed light green).

1. V_a corresponds to the potential V with the part proportional to the logarithm neglected. V_a exactly overlaps with the full potential (solid blue line).

2. V_b corresponds to the potential V with the choice of $\mu = \varphi$ (darkest green, long-dashed line). This choice alone does not modify the potential significantly with respect to our choice (solid blue line).

3. V_c corresponds to the potential V with the constant $-\frac{5}{6}$ neglected (dark green, medium-dashed curve). Since the omission of the logarithm (with our choice of the scale) does not visibly modify the result, V_c is equivalent to using the tree-level part of V. Here the difference with respect to the full potential is significant. It is understandable, since the choice of the scale was such as to get rid of the logarithmic term but not the $\frac{5}{6}$ constant.

4. V_d corresponds to the tree-level part of V but with the choice $\mu = \varphi$ (light green, short-dashed line), which makes this choice very close to V_1 and V_2 discussed above. Clearly, V_d differs significantly from the full potential.

5. Phase transition and gravitational wave signal

A first-order phase transition proceeds through nucleation, growth and percolation of bubbles filled with the broken-symmetry phase in the sea of the symmetric phase. This corresponds to the fields tunnelling through a potential barrier. In our case, we have checked that tunnelling proceeds along the φ direction, while the transition in the h direction is smooth.

5.1 Important temperatures

The temperatures relevant to our discussion are:

PoS(CORFU2022)106

Critical Temperature T_c. At high temperatures the symmetry is restored and the effective potential has a single minimum at the origin of the field space. As the Universe cools down, a second minimum is formed. At the critical temperature, the two minima are degenerate, and for lower temperatures, the minimum with broken symmetry becomes the true vacuum. This is the temperature at which the tunnelling becomes possible.

Thermal Inflation Temperature T_V. If there is large supercooling, i.e. the phase transition is delayed to low temperatures, much below the critical temperature, it is possible that a period of thermal inflation due to the false vacuum energy appears before the phase transition completes. The Hubble parameter can be written as

$$H^2 = \frac{1}{3\bar{M}_{\rm Pl}^2}(\rho_R + \rho_V) = \frac{1}{3\bar{M}_{\rm Pl}^2}\left(\frac{T^4}{\xi_g^2} + \Delta V\right), \quad \xi_g = \sqrt{30/(\pi^2 g_*)}, \tag{5.1}$$

where ΔV is the difference between the values of the effective potential at false and true vacuum. The onset of the period of thermal inflation can be approximately attributed to the temperature at which vacuum and radiation contribute to the energy density equally,

$$T_V \equiv \left(\xi_g^2 \Delta V\right)^{\frac{1}{4}}. \tag{5.2}$$

For supercooled transitions, it is a good approximation to assume that ΔV is independent of the temperature below T_V. By using the temperature T_V, the Hubble constant can be rewritten as

$$H^2 \simeq \frac{1}{3\bar{M}_{\rm Pl}^2 \xi_g^2}\left(T^4 + T_V^4\right). \tag{5.3}$$

In the case of large supercooling, the contribution to the Hubble parameter from radiation energy can be neglected, leaving

$$H^2 \simeq H_V^2 = \frac{1}{3\bar{M}_{\rm Pl}^2}\Delta V. \tag{5.4}$$

In figure 3 there are the same excluded areas as before and two new shaded regions. The lower left corner (darkest grey) is not analysed because there the PT is sourced by the QCD phase transition, which is beyond the scope of the present work. The light-grey region around $M_X \approx 10^6\,$GeV is where the percolation criterion of eq. (5.13) is violated and is discussed in more detail below.

Nucleation Temperature T_n. Below the critical temperature, nucleation of bubbles of true vacuum becomes possible. To compute the decay rate of the false vacuum we start by solving the bounce equation,

$$\frac{{\rm d}^2\varphi}{{\rm d}r^2} + \frac{2}{r}\frac{{\rm d}\varphi}{{\rm d}r} = \frac{{\rm d}V(\varphi,T)}{{\rm d}\varphi}, \qquad \frac{{\rm d}\varphi}{{\rm d}r} = 0 \quad \text{for} \quad r = 0 \quad \text{and} \quad \varphi \to 0 \quad \text{for} \quad r \to \infty. \tag{5.5}$$

Once the bubble profile is known we can compute the Euclidean action along the tunnelling path

$$S_3(T) = 4\pi \int r^2 {\rm d}r \frac{1}{2}\left(\frac{{\rm d}\varphi}{{\rm d}r}\right)^2 + V(\varphi,T). \tag{5.6}$$

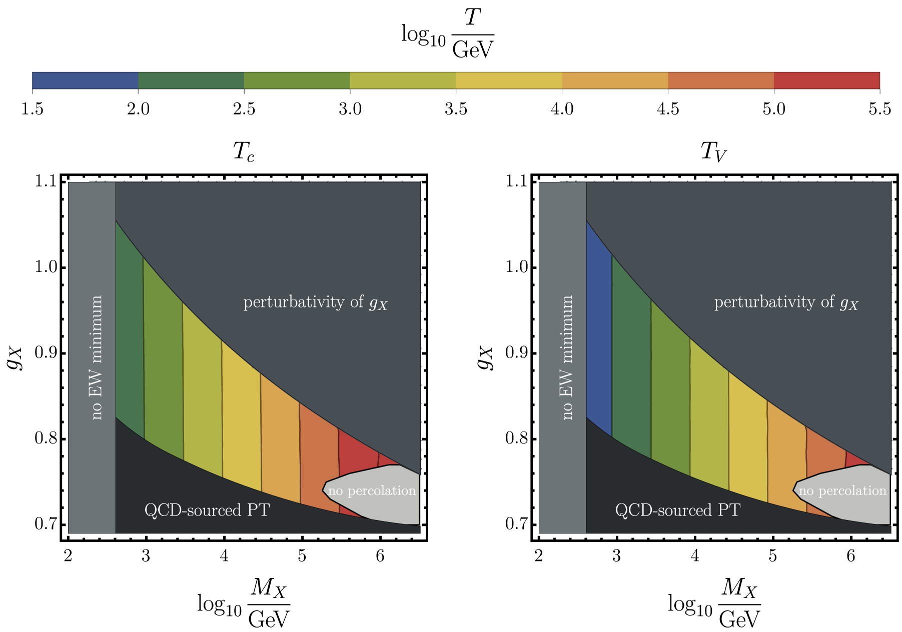

Figure 3: The values of the critical temperature T_c (left panel) and the temperature at which thermal inflation starts T_V (right panel).

Then the decay rate of the false vacuum due to the thermal fluctuations is given by

$$\Gamma(T) \approx T^4 \left(\frac{S_3(T)}{2\pi T}\right)^{3/2} e^{-S_3(T)/T}. \tag{5.7}$$

The nucleation temperature is defined as the temperature at which at least one bubble is nucleated per Hubble volume, which can be interpreted as the onset of the PT.

$$N(T_n) = 1 = \int_{t_c}^{t_n} dt \frac{\Gamma(t)}{H(t)^3} = \int_{T_n}^{T_c} \frac{dT}{T} \frac{\Gamma(T)}{H(T)^4}. \tag{5.8}$$

The common criterion for evaluating T_n as $S_3/T_n \approx 140$ is not reliable in the case of strongly supercooled transitions.

Percolation Temperature T_p. When the bubbles of the true vacuum percolate, most of the bubble collisions take place. Therefore, the percolation temperature is the relevant temperature for the GW signal generation. The probability of finding a point still in the false vacuum at a certain temperature is given by $P(T) = e^{-I(T)}$, where $I(T)$ is the amount of true vacuum volume per unit comoving volume and reads as

$$I(T) = \frac{4\pi}{3} \int_T^{T_c} \mathrm{d}T' \frac{\Gamma(T')}{T'^4 H(T')} \left(\int_T^{T'} \frac{\mathrm{d}\tilde{T}}{H(\tilde{T})}\right)^3. \tag{5.9}$$

We can distinguish between the vacuum and radiation domination period which leads to the Hubble parameter in the following form:

$$H(T) \simeq \begin{cases} H_\mathrm{R}(T) = \frac{T^2}{\sqrt{3}\bar{M}_\mathrm{pl}\xi_g}, & \text{for} \quad T > T_V, \\ H_\mathrm{V} = \frac{T_V^2}{\sqrt{3}\bar{M}_\mathrm{pl}\xi_g}, & \text{for} \quad T < T_V. \end{cases} \tag{5.10}$$

We can thus write a simplified version of $I(T)$ valid in the region where $T < T_V$:

$$I_{\rm RV}(T) = \frac{4\pi}{3H_{\rm V}^4}\left(\int_{T_V}^{T_c}\frac{dT'\Gamma(T')}{T'^6}T_V^2\left(2T_V - T - \frac{T_V^2}{T'}\right)^3 + \int_{T}^{T_V}\frac{dT'\Gamma(T')}{T'}\left(1-\frac{T}{T'}\right)^3\right) \tag{5.11}$$

The percolation criterion is given by [148]

$$I_{\rm RV}(T_p) = 0.34\,, \qquad \text{or} \qquad P(T_p) = 0.7\,. \tag{5.12}$$

The fraction 0.34 is the ratio of the volume in equal-size and randomly-distributed spheres (including overlapping regions) to the total volume of space for which percolation occurs in three-dimensional Euclidean space, and implies that at T_p at least 34% of the (comoving) volume is converted to the true minimum.

Comparing to the values of T_n (fig. 4) one can see that these two temperatures are of the same order, yet they differ, hence one should not use T_n as a proxy for the temperature at which the PT proceeds in case of the models with large supercooling.

One also needs to make sure that the volume of the false vacuum $V_f \sim a^3(T)P(T)$ is decreasing around the percolation temperature. This condition is especially constraining in models featuring strong supercooling, as thermal inflation can prevent bubbles from percolating. It can be expressed as

$$\frac{1}{V_f}\frac{{\rm d}V_f}{{\rm d}t} = 3H(t) - \frac{{\rm d}I(t)}{{\rm d}t} = H(T)\left(3 + T\frac{{\rm d}I(T)}{{\rm d}T}\right) < 0. \tag{5.13}$$

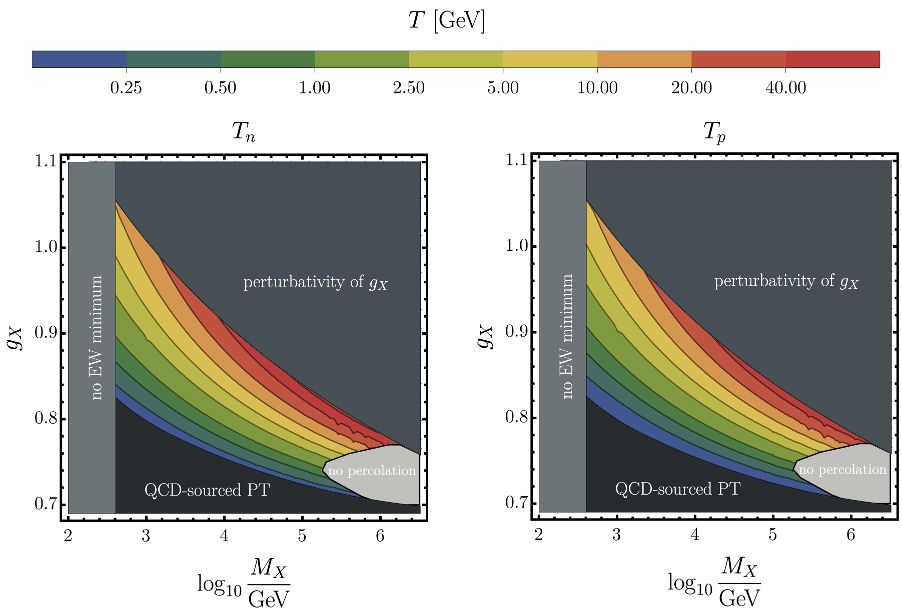

Figure 4: The values of the nucleation temperature T_n (left panel) and the percolation temperature T_p (right panel).

Reheating Temperature T_r. At the end of the phase transition, the Universe is in a vacuum-dominated state. Then the total energy released in the phase transition is $\Delta V(T_p) \approx \Delta V(T = 0) \equiv \Delta V$. If reheating is instantaneous, this whole energy is turned into the energy of radiation,

$$\Delta V = \rho_R(T_r) = \rho_R(T_V) \qquad \to \qquad T_r = T_V. \tag{5.14}$$

On the other hand, if at T_p the rate of energy transfer from the φ field to the plasma, Γ_φ, is smaller than the Hubble parameter, $\Gamma_\varphi < H(T_p)$, then the energy will be stored in the scalar field oscillating about the true vacuum and redshift as matter until Γ_φ becomes comparable to the Hubble parameter. In this case

$$T_r = T_V \sqrt{\frac{\Gamma_\varphi}{H_*}}. \tag{5.15}$$

The rate of energy transfer from φ to the plasma reads

$$\Gamma_\varphi = \xi_S^2(1-\xi_S^2)\Gamma_{\rm SM}(S) + (1-\xi_S^2)\Gamma(S \to HH), \quad \xi_S = \begin{cases} -\sin\theta & \text{for } M_H \leqslant M_S \\ \cos\theta & \text{for } M_H > M_S \end{cases} \tag{5.16}$$

where $\Gamma_{\rm SM}$ denotes a decay width computed as in the SM, i.e. with the same couplings and decay channels, but for a particle of mass M_S. The mixing enhances the decay width twofold, first, it amplifies the coupling SHH as compared to φhh and, moreover, it allows a contribution from the SM sector, which is especially important when the $S \to HH$ decay is kinematically forbidden.

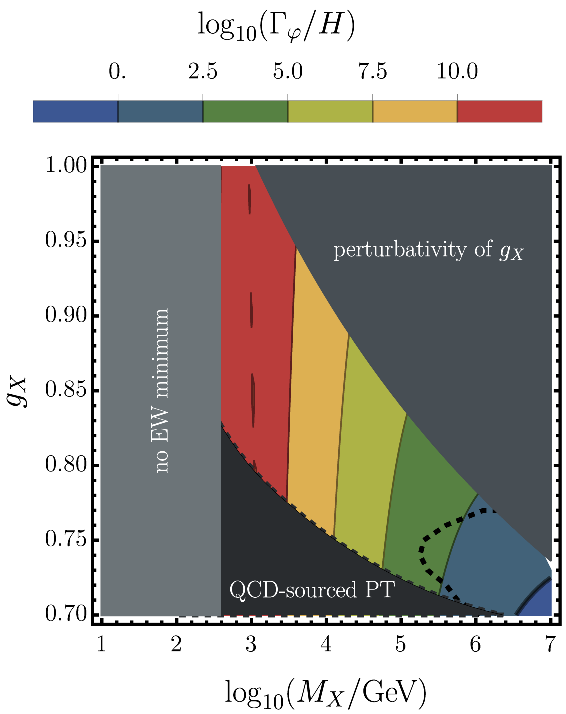

Figure 5: Contour plot of the decimal logarithm of the ratio of the energy transfer rate Γ_φ to the Hubble parameter H. The equality $H = \Gamma_\varphi$ is indicated as a thick black solid line in the lower right corner. The percolation bound is shown as a black dashed line (in other plots it is shown as a light-grey region).

5.2 Supercool Dark Matter?

The authors of [31, 64, 76] claim that for a wide range of parameters, there can be supercool DM. Their main assumptions are:

- The true vacuum has zero energy, the energy in the false vacuum is $\Delta V \simeq 9m_\chi^4/(128\pi^2)$, which implies that supercooling starts at

$$T_V \simeq \frac{M_X}{8.5} \quad \text{and} \quad H_* = \sqrt{\frac{3}{\pi}}\frac{M_X^2}{4M_{\rm pl}}\,.$$

- Nucleation occurs when $S_3(T_n)/T_n \simeq 4\ln\big(M_{\rm pl}/m_\chi\big) \simeq 142$.

- The reheating temperature is related to the thermal inflation temperature as $T_{\rm r} = T_V\ \min\left(1, \Gamma/H\right)^{1/2}$, where $\Gamma \simeq \Gamma_h \sin^2(v/w)$, with $\Gamma_h \approx 4$ MeV.

- The DM abundance resulting from inflationary supercooling is

$$Y_{\rm DM} \equiv \frac{n_{\rm DM}|_{T=T_{\rm r}}}{s|_{T=T_{\rm r}}} = \frac{45 g_{\rm DM}}{2\pi^4 g_*}\frac{T_{\rm r}}{T_{\rm V}}\left(\frac{T_{\rm n}}{T_{\rm V}}\right)^3\,.$$

- For $T_{\rm r} < T_{\rm dec} \simeq M_X/25$, both supercooling and sub-thermal production contribute to the DM relic abundance,

$$\Omega_{\rm DM}h^2 = \Omega_{\rm DM}h^2|_{\rm supercool} + \Omega_{\rm DM}h^2|_{\rm sub-thermal}\,.$$

- For $T_{\rm r} > T_{\rm dec}$, the plasma thermalizes again, and the usual freeze-out mechanism yields the relic abundance,

$$\Omega_{\rm DM}h^2 = \Omega_{\rm DM}h^2|_{\rm freeze-out}\,.$$

Nevertheless, our analysis suggests that due to the percolation criterion which excludes M_X above $\sim 10^6$ GeV and the fact that $\Gamma_\varphi > H(T_p)$ in the rest of the DM range, we find $T_r > T_{\rm dec}$ for all parameter points. Hence, the supercool DM population gets diluted away, the sub-thermal population reaches thermal equilibrium again, and the relic abundance is produced as in the standard freezeout scenario (see fig. 6). Our conclusions were also validated in a recent paper [153].

5.3 Gravitational waves

The GW signal in the model under consideration can be sourced by bubble collisions. The spectrum is:

$$\Omega_{\rm col}(f) = \left(\frac{R_* H_*}{5}\right)^2\left(\frac{\kappa_{\rm col}\alpha}{1+\alpha}\right)^2 S_{\rm col}(f)\,. \tag{5.17}$$

where R_* is the length scale of the transition, $\kappa_{\rm col}$ is the energy transfer efficiency factor at the end of the transition and $\alpha = \Delta V/\rho_R(T_p)$ is the transition strength. The spectral shape $S_{\rm col}$ and peak frequency are defined as

$$S_{\rm col} = 25.09\left[2.41\left(\frac{f}{f_{\rm col}}\right)^{-0.56} + 2.34\left(\frac{f}{f_{\rm col}}\right)^{0.57}\right]^{-4.2}\,, \qquad f_{\rm col} \simeq 0.13\left(\frac{5}{R_* H_*}\right)\,. \tag{5.18}$$

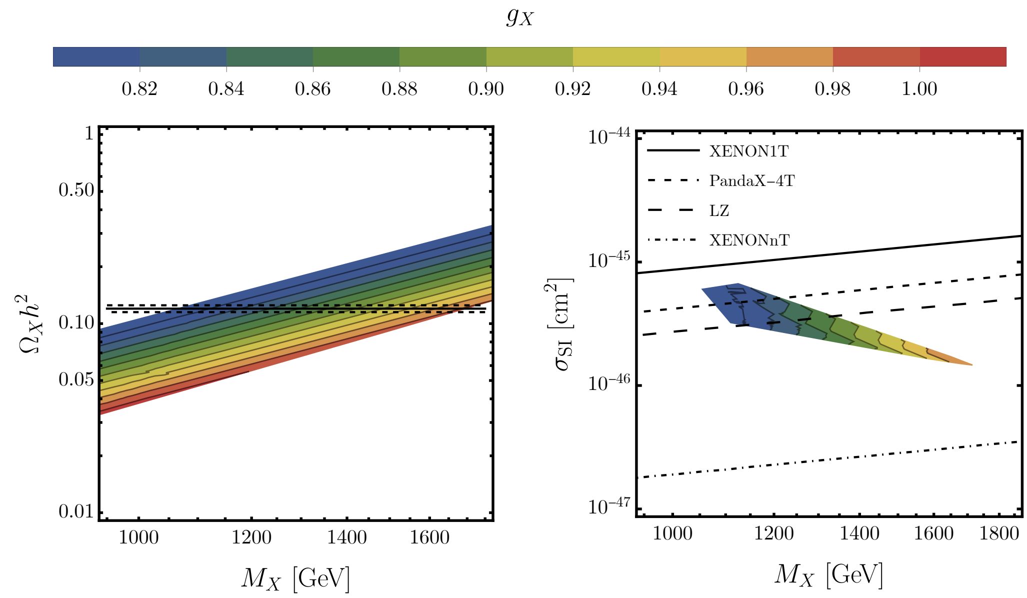

Figure 6: Left: Dark matter relic abundance $\Omega_X h^2$ with colour changing according to the value of the gauge coupling g_X. The black lines correspond to the measured value $\Omega_{\rm DM} h^2 = 0.120 \pm 5\sigma$. Right: The spin-independent dark matter-nucleon cross section. The coloured region corresponds to points that reproduce the measured relic abundance within 5σ. The lines represent the exclusion limit from the XENON1T 2018 [149] (solid), PandaX-4T 2021 [150] (dashed), LZ 2022 [151] (large dashed) and the scheduled XENONnT [152] (dot dashed) experiments.

The spectra of the sound-wave-sourced GW are expressed as:

$$\Omega_{\rm sw}(f) = \left(\frac{R_* H_*}{5}\right)\left(1 - \frac{1}{\sqrt{1+2\tau_{\rm sw} H_*}}\right)\left(\frac{\kappa_{\rm sw}\alpha}{1+\alpha}\right)^2 S_{\rm sw}(f), \tag{5.19}$$

with

$$S_{\rm sw}(f) = \left(\frac{f}{f_{\rm sw}}\right)^3 \left[\frac{4}{7} + \frac{3}{7}\left(\frac{f}{f_{\rm sw}}\right)^2\right]^{7/2}, \tag{5.20}$$

where the duration of the sound wave period normalised to Hubble and the peak frequency can be expressed as

$$\tau_{\rm sw} H_* = \frac{R * H_*}{U_f}, \quad U_f \simeq \sqrt{\frac{3}{4}\frac{\alpha}{1+\alpha}\kappa_{\rm sw}}, \quad f_{\rm sw} \simeq 0.54\left(\frac{5}{R_* H_*}\right). \tag{5.21}$$

To assess the observability of a signal we compute the signal-to-noise (SNR) ratio for the detectors that have the best potential of observing the predicted signal, i.e. LISA and AEDGE. We calculate the SNR using the usual formula [154, 155]:

$$\text{SNR} = \sqrt{\mathscr{T} \int_{f_{\rm min}}^{f_{\rm max}} \mathrm{d}f \left[\frac{h^2 \Omega_{\rm GW}(f)}{h^2 \Omega_{\rm Sens}(f)}\right]^2}, \tag{5.22}$$

where $\mathscr{T}$ is the duration of collecting data and $h^2\Omega_{\rm Sens}(f)$ is the sensitivity curve of a given detector. For calculations we have used data collecting durations as $\mathscr{T}_{\rm LISA} = 75\ \% \cdot 4$ years [154] and $\mathscr{T}_{\rm AEDGE} = 3$ years [17]. We will assume that a signal could be observed if SNR > 10, which is the usual criterion.

The results are presented in figure 7. Superimposed is a curve indicating where in the parameter space the correct DM relic density is reproduced and the DM direct detection constraints are satisfied (solid black). Strikingly, the SNR for LISA for the predicted signal is above the observability threshold within the whole parameter space, and almost whole in the case of AEDGE. This means that a first-order phase transition sourced by tunnelling of a scalar field in the present model should be thoroughly testable by LISA and AEDGE. Moreover, in case of not observing a signal consistent with the expectations for the first-order phase transitions this scenario could be falsified.

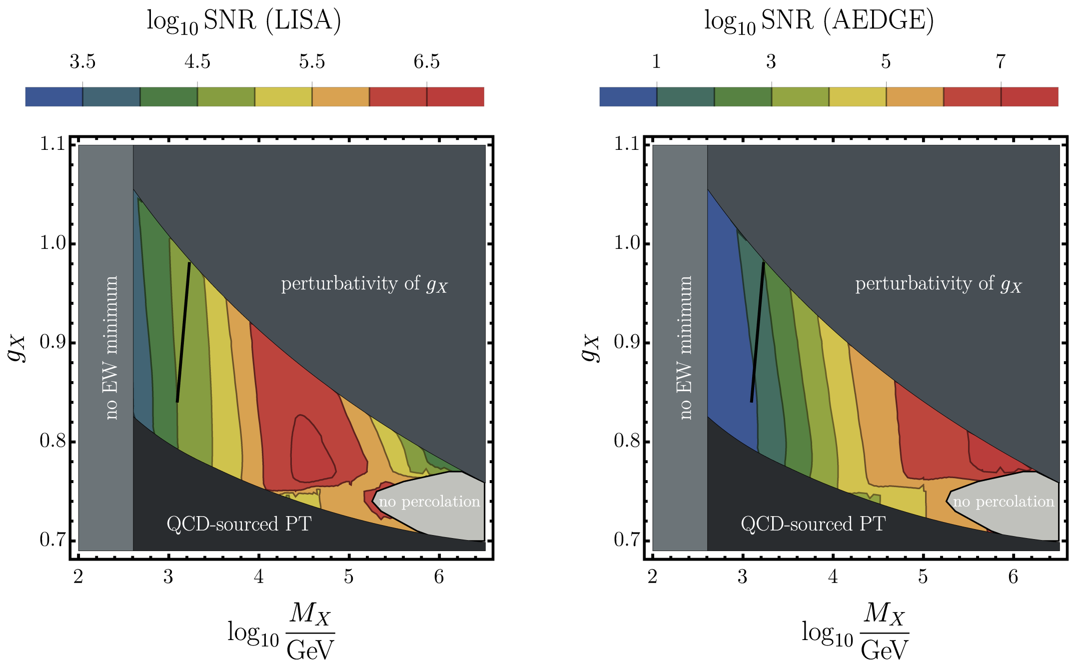

Figure 7: Results for the signal-to-noise ratio for LISA (left panel) and AEDGE (right panel) for the predicted GW signal. The black line corresponds to the points that reproduce the measured DM relic abundance and also evade the DM direct detection experimental constraints.

The correct DM relic abundance and non-exclusion by direct detection experiments (solid black line in figure 7) are located in the region of a relatively weaker signal. It is still well observable with LISA and AEDGE. The GW signal in the region where the correct abundance is reproduced is sourced entirely by sound waves. Examples of spectra for points along the black line in figure 7 are shown in figure 8.

5.4 Renormalisation-scale dependence

Finally, we perform scans of the parameter space at fixed μ. This will tell us how our understanding of the parameter space and observability of the GW signal depends on the renormalisation

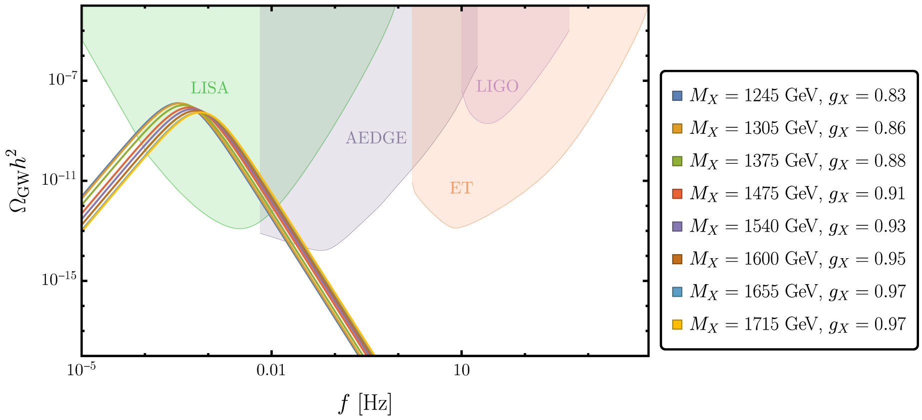

Figure 8: Predictions for spectra of gravitational waves together with integrated sensitivity curves for LISA, AEDGE, ET and LIGO for the points in the parameter space where DM relic abundance is saturated.

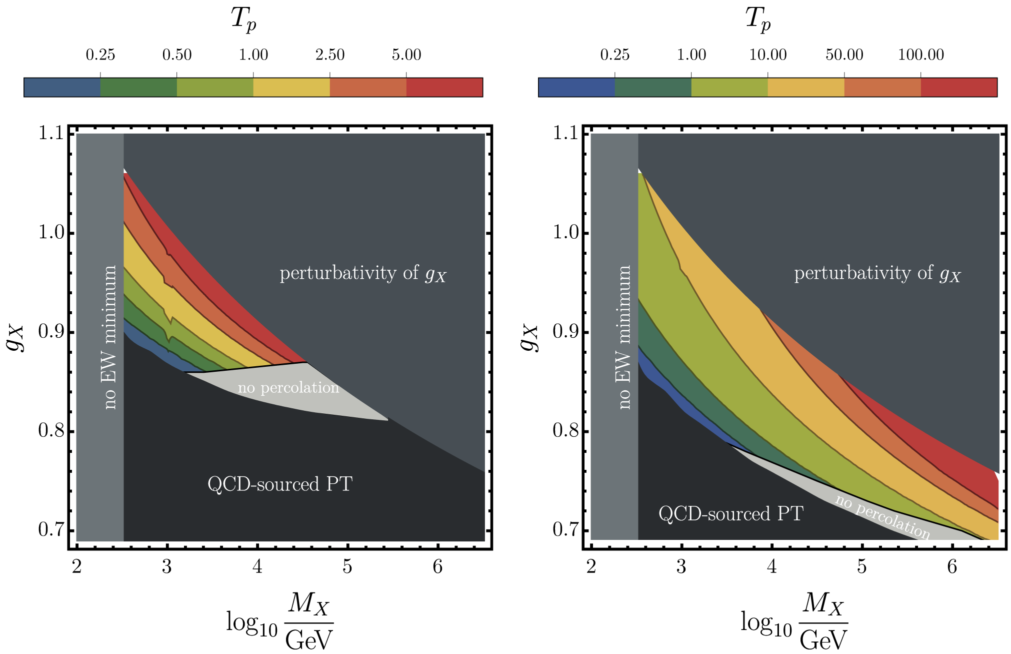

Figure 9: Results of the scan with fixed renormalisation scale, $\mu = M_X$ (left), $\mu = M_Z$ (right) for the percolation temperature T_p.

scale. Figure 9 shows the results for the percolation temperature T_p computed at different scales ($\mu = M_X$ (left), $\mu = M_Z$ (right)) together with the previous constraints on the parameter space. Both figures indicate a striking dependence on the renormalisation scale. This has further implications since for $T_p \lesssim 0.1\,$GeV the PT is believed to be sourced by the QCD effects, which changes the nature and properties of the PT. In this work we focus on the PT sourced by the tunnelling, therefore the considered parameter space changes dramatically as the renormalisation scale is changed. Also, the answer to a basic question – whether or not the PT completes via percolation of bubbles of the true vacuum – is altered by the change of the renormalisation scale as can be seen by examining the percolation criterion (light-grey shaded region). The results show that the change of the scale at which computations are performed not only changes the results quantitatively, by shifting the values of the characteristic parameters of the phase transition, but it also significantly modifies them qualitatively – by modifying the character of the phase transition, the very fact of its completion and the dominant source of the GW signal.

6. Summary and conclusions

In the present work, we studied a model endowed with classical scale invariance, a dark $SU(2)_X$ gauge group and a scalar doublet of this group. This model provides a dynamical mechanism of generating all the mass scales via radiative symmetry breaking, while featuring only two free parameters. Moreover, it provides dark matter candidates – the three gauge bosons of the $SU(2)_X$ group which are degenerate in mass – stabilised by an intrinsic $\mathbb{Z}_2 \times \mathbb{Z}_2'$ symmetry. Like other models with scaling symmetry, the studied model exhibits strong supercooling which results in the generation of an observable gravitational-wave signal.

Motivated by these attractive features we performed an analysis of the phase transition, gravitational wave generation and dark matter relic abundance, updating and extending the existing results [25, 31, 32, 50, 64, 71–76]. The analysis features the key ingredients:

- careful analysis of the potential in the light of radiative symmetry breaking;
- using renormalisation-group improved potential which includes all the leading order terms;
- using RG-running to move between various relevant scales: the electroweak scale for scalar mass generation, the scale of the mass of the new scalar for its decay during reheating;
- careful analysis of the supercooled phase transition, following recent developments, in particular imposing the percolation criterion which proved crucial for phenomenological predictions;
- analysis of dark matter relic abundance in the light of the updated picture of the phase transition;
- analysis of gravitational-wave spectra using most recent results from simulations;
- using fixed-scale potential, in addition to the renormalisation-group-improved one, to study the scale dependence of the results.

The first and foremost result of our analysis is that within the model the gravitational wave signal sourced by a first-order phase transition associated with the $SU(2)_X$ and electroweak symmetry breaking is strong and observable for the whole allowed parameter space. This is an important conclusion since it allows this scenario to be falsified in case of negative LISA results.

Second, we exclude the supercool dark matter scenario within the region where the phase transition proceeds via nucleation and percolation of bubbles of the true vacuum. It is a result of a combination of two reasons: we include the percolation condition, eq. (5.13), which allows to verify that a strongly supercooled phase transition indeed completes via percolation of bubbles and strongly constrains the parameter space relevant for our analysis. Moreover, we improve on the computation of the decay rate of the scalar field φ, which controls the reheating rate, which pushes the onset of inefficient reheating towards higher M_X, beyond the region of interest.

Third, we find the parameter space in which the correct relic dark matter abundance is predicted. It is produced via the standard freeze-out mechanism in the region with relatively low M_X and large g_X. It is the region where the phase transition is relatively weak (compared with other regions of the parameter space), yet the gravitational-wave signal should be well observable with LISA. This parameter space is further reduced due to the recent direct detection constraints.

Moreover, in the present work we focused on the issue of scale dependence of the predictions. Our approach to reducing this dependence was to implement the renormalisation-group improvement procedure, respecting the power counting of couplings to include all the relevant terms. For comparison, we present results of computations performed at fixed scale, where the dependence on the renormalisation scale is significant. It is important to note that with the change of the scale the predictions do not only change quantitatively, they can change qualitatively. For example, for computations performed at a fixed scale (both $\mu = M_X$ and M_Z) gravitational waves sourced by bubble collisions are not present. At the same time, with RG improvement we see a substantial region where bubble collisions are efficient in producing an observable signal.

To sum up, the classically scale-invariant model with an extra SU(2) symmetry remains a valid theoretical framework for describing dark matter and gravitational-wave signal produced during a first-order phase transition in the early Universe. It will be tested experimentally by LISA and other gravitational-wave detectors. The predictions, however, are sensitive to the theoretical procedures implemented. Therefore, it is crucial to improve our understanding of theoretical pitfalls affecting the predictions. The present work is a step in this direction.

Acknowledgments

We would like to thank Kristjan Kannike, Wojciech Kotlarski, Luca Marzola, Tania Robens, Martti Raidal and Rui Santos for useful discussions. We are indebted to Marek Lewicki for numerous discussions, clarifications and sharing data for the SNR plots. We are grateful to João Viana for his computation of Higgs decay width using `hdecay` and IT hints. We would also like to thank Matti Heikinheimo, Tomislav Prokopec, Tommi Tenkanen, Kimmo Tuominen and Ville Vaskonen for collaboration in the early stages of this work. AK was supported by the Estonian Research Council grants MOBTT5, MOBTT86, PSG761 and by the EU through the European Regional Development Fund CoE program TK133 "The Dark Side of the Universe". The work of BŚ and MK is supported by the National Science Centre, Poland, through the SONATA project number 2018/31/D/ST2/03302. AK would also like the thank the organizers of the "School and Workshops on Elementary Particle Physics and Gravity", Corfu 2022, for their hospitality during his stay, and for giving him the opportunity to present this work.

References

[1] M. Kierkla, A. Karam, and B. Swiezewska, "Conformal model for gravitational waves and dark matter: a status update," JHEP **03** (2023) 007, `arXiv:2210.07075 [astro-ph.CO]`.

[2] **Virgo, LIGO Scientific** Collaboration, B. P. Abbott et al., "Observation of Gravitational Waves from a Binary Black Hole Merger," Phys. Rev. Lett. **116** no.~6, (2016) 061102, arXiv:1602.03837 [gr-qc].

[3] **Virgo, LIGO Scientific** Collaboration, B. P. Abbott et al., "GW151226: Observation of Gravitational Waves from a 22-Solar-Mass Binary Black Hole Coalescence," Phys. Rev. Lett. **116** no.~24, (2016) 241103, arXiv:1606.04855 [gr-qc].

[4] **VIRGO, LIGO Scientific** Collaboration, B. P. Abbott et al., "GW170104: Observation of a 50-Solar-Mass Binary Black Hole Coalescence at Redshift 0.2," Phys. Rev. Lett. **118** no.~22, (2017) 221101, arXiv:1706.01812 [gr-qc]. [Erratum: Phys. Rev. Lett.121,no.12,129901(2018)].

[5] **Virgo, LIGO Scientific** Collaboration, B. Abbott et al., "GW170817: Observation of Gravitational Waves from a Binary Neutron Star Inspiral," Phys. Rev. Lett. **119** no.~16, (2017) 161101, arXiv:1710.05832 [gr-qc].

[6] **LIGO Scientific, Virgo** Collaboration, B. P. Abbott et al., "GW170814: A Three-Detector Observation of Gravitational Waves from a Binary Black Hole Coalescence," Phys. Rev. Lett. **119** no.~14, (2017) 141101, arXiv:1709.09660 [gr-qc].

[7] **LIGO Scientific, Virgo** Collaboration, B. . P. . Abbott et al., "GW170608: Observation of a 19-solar-mass Binary Black Hole Coalescence," Astrophys. J. Lett. **851** (2017) L35, arXiv:1711.05578 [astro-ph.HE].

[8] N. Bartolo et al., "Science with the space-based interferometer LISA. IV: Probing inflation with gravitational waves," JCAP **12** (2016) 026, arXiv:1610.06481 [astro-ph.CO].

[9] C. Caprini, D. G. Figueroa, R. Flauger, G. Nardini, M. Peloso, M. Pieroni, A. Ricciardone, and G. Tasinato, "Reconstructing the spectral shape of a stochastic gravitational wave background with LISA," JCAP **11** (2019) 017, arXiv:1906.09244 [astro-ph.CO].

[10] C. Gowling and M. Hindmarsh, "Observational prospects for phase transitions at LISA: Fisher matrix analysis," JCAP **10** (2021) 039, arXiv:2106.05984 [astro-ph.CO].

[11] **LISA Cosmology Working Group** Collaboration, P. Auclair et al., "Cosmology with the Laser Interferometer Space Antenna," arXiv:2204.05434 [astro-ph.CO].

[12] G. Boileau, N. Christensen, C. Gowling, M. Hindmarsh, and R. Meyer, "Prospects for LISA to detect a gravitational-wave background from first order phase transitions," arXiv:2209.13277 [gr-qc].

[13] C. Gowling, M. Hindmarsh, D. C. Hooper, and J. Torrado, "Reconstructing physical parameters from template gravitational wave spectra at LISA: first order phase transitions," arXiv:2209.13551 [astro-ph.CO].

[14] L. Badurina et al., "AION: An Atom Interferometer Observatory and Network," JCAP **05** (2020) 011, arXiv:1911.11755 [astro-ph.CO].

[15] P. W. Graham, J. M. Hogan, M. A. Kasevich, and S. Rajendran, "Resonant mode for gravitational wave detectors based on atom interferometry," Phys. Rev. D **94** no.~10, (2016) 104022, arXiv:1606.01860 [physics.atom-ph].

[16] **MAGIS** Collaboration, P. W. Graham, J. M. Hogan, M. A. Kasevich, S. Rajendran, and R. W. Romani, "Mid-band gravitational wave detection with precision atomic sensors," arXiv:1711.02225 [astro-ph.IM].

[17] **AEDGE** Collaboration, Y. A. El-Neaj et al., "AEDGE: Atomic Experiment for Dark Matter and Gravity Exploration in Space," EPJ Quant. Technol. **7** (2020) 6, arXiv:1908.00802 [gr-qc].

[18] M. Punturo et al., "The Einstein Telescope: A third-generation gravitational wave observatory," Class. Quant. Grav. **27** (2010) 194002.

[19] S. Hild et al., "Sensitivity Studies for Third-Generation Gravitational Wave Observatories," Class. Quant. Grav. **28** (2011) 094013, arXiv:1012.0908 [gr-qc].

[20] **LIGO Scientific** Collaboration, G. M. Harry, "Advanced LIGO: The next generation of gravitational wave detectors," Class. Quant. Grav. **27** (2010) 084006.

[21] **VIRGO** Collaboration, F. Acernese et al., "Advanced Virgo: a second-generation interferometric gravitational wave detector," Class. Quant. Grav. **32** no.~2, (2015) 024001, arXiv:1408.3978 [gr-qc].

[22] **LIGO Scientific** Collaboration, J. Aasi et al., "Advanced LIGO," Class. Quant. Grav. **32** (2015) 074001, arXiv:1411.4547 [gr-qc].

[23] **LIGO Scientific, Virgo** Collaboration, R. Abbott et al., "Open data from the first and second observing runs of Advanced LIGO and Advanced Virgo," SoftwareX **13** (2021) 100658, arXiv:1912.11716 [gr-qc].

[24] C. Caprini et al., "Science with the space-based interferometer eLISA. II: Gravitational waves from cosmological phase transitions," JCAP **1604** no.~04, (2016) 001, arXiv:1512.06239 [astro-ph.CO].

[25] T. Hambye and A. Strumia, "Dynamical generation of the weak and Dark Matter scale," Phys. Rev. **D88** (2013) 055022, arXiv:1306.2329 [hep-ph].

[26] J. Jaeckel, V. V. Khoze, and M. Spannowsky, "Hearing the signal of dark sectors with gravitational wave detectors," Phys. Rev. **D94** no.~10, (2016) 103519, arXiv:1602.03901 [hep-ph].

[27] K. Hashino, M. Kakizaki, S. Kanemura, and T. Matsui, "Synergy between measurements of gravitational waves and the triple-Higgs coupling in probing the first-order electroweak phase transition," Phys. Rev. **D94** no.~1, (2016) 015005, arXiv:1604.02069 [hep-ph].

[28] R. Jinno and M. Takimoto, "Probing a classically conformal B-L model with gravitational waves," Phys. Rev. **D95** no.~1, (2017) 015020, arXiv:1604.05035 [hep-ph].

[29] L. Marzola, A. Racioppi, and V. Vaskonen, "Phase transition and gravitational wave phenomenology of scalar conformal extensions of the Standard Model," Eur. Phys. J. **C77** no.~7, (2017) 484, arXiv:1704.01034 [hep-ph].

[30] P. H. Ghorbani, "Electroweak phase transition in the scale invariant standard model," Phys. Rev. D **98** no.~11, (2018) 115016, arXiv:1711.11541 [hep-ph].

[31] I. Baldes and C. Garcia-Cely, "Strong gravitational radiation from a simple dark matter model," JHEP **05** (2019) 190, arXiv:1809.01198 [hep-ph].

[32] T. Prokopec, J. Rezacek, and B. Świeżewska, "Gravitational waves from conformal symmetry breaking," JCAP **02** (2019) 009, arXiv:1809.11129 [hep-ph].

[33] C. Marzo, L. Marzola, and V. Vaskonen, "Phase transition and vacuum stability in the classically conformal B–L model," Eur. Phys. J. C **79** no.~7, (2019) 601, arXiv:1811.11169 [hep-ph].

[34] A. Mohamadnejad, "Gravitational waves from scale-invariant vector dark matter model: Probing below the neutrino-floor," Eur. Phys. J. C **80** no.~3, (2020) 197, arXiv:1907.08899 [hep-ph].

[35] A. Ghoshal and A. Salvio, "Gravitational waves from fundamental axion dynamics," JHEP **12** (2020) 049, `arXiv:2007.00005 [hep-ph]`.

[36] Z. Kang and J. Zhu, "Scale-genesis by Dark Matter and Its Gravitational Wave Signal," Phys. Rev. D **102** no.~5, (2020) 053011, `arXiv:2003.02465 [hep-ph]`.

[37] A. Mohamadnejad, "Electroweak phase transition and gravitational waves in a two-component dark matter model," JHEP **03** (2022) 188, `arXiv:2111.04342 [hep-ph]`.

[38] A. Dasgupta, P. S. B. Dev, A. Ghoshal, and A. Mazumdar, "Gravitational Wave Pathway to Testable Leptogenesis," `arXiv:2206.07032 [hep-ph]`.

[39] R. Hempfling, "The Next-to-minimal Coleman-Weinberg model," Phys. Lett. **B379** (1996) 153–158, `arXiv:hep-ph/9604278 [hep-ph]`.

[40] M. Sher, "The Coleman-Weinberg phase transition in extended Higgs models," Phys. Rev. D **54** (1996) 7071–7074, `arXiv:hep-ph/9607337`.

[41] W.-F. Chang, J. N. Ng, and J. M. S. Wu, "Shadow Higgs from a scale-invariant hidden U(1)(s) model," Phys. Rev. **D75** (2007) 115016, `arXiv:hep-ph/0701254 [HEP-PH]`.

[42] S. Iso, N. Okada, and Y. Orikasa, "Classically conformal $B-L$ extended Standard Model," Phys. Lett. **B676** (2009) 81–87, `arXiv:0902.4050 [hep-ph]`.

[43] S. Iso and Y. Orikasa, "TeV Scale B-L model with a flat Higgs potential at the Planck scale: In view of the hierarchy problem," PTEP **2013** (2013) 023B08, `arXiv:1210.2848 [hep-ph]`.

[44] C. Englert, J. Jaeckel, V. V. Khoze, and M. Spannowsky, "Emergence of the Electroweak Scale through the Higgs Portal," JHEP **04** (2013) 060, `arXiv:1301.4224 [hep-ph]`.

[45] V. V. Khoze and G. Ro, "Leptogenesis and Neutrino Oscillations in the Classically Conformal Standard Model with the Higgs Portal," JHEP **10** (2013) 075, `arXiv:1307.3764 [hep-ph]`.

[46] V. V. Khoze, "Inflation and Dark Matter in the Higgs Portal of Classically Scale Invariant Standard Model," JHEP **11** (2013) 215, `arXiv:1308.6338 [hep-ph]`.

[47] M. Hashimoto, S. Iso, and Y. Orikasa, "Radiative symmetry breaking at the Fermi scale and flat potential at the Planck scale," Phys. Rev. D **89** no.~1, (2014) 016019, `arXiv:1310.4304 [hep-ph]`.

[48] M. Hashimoto, S. Iso, and Y. Orikasa, "Radiative symmetry breaking from flat potential in various U(1)' models," Phys. Rev. D **89** no.~5, (2014) 056010, `arXiv:1401.5944 [hep-ph]`.

[49] S. Benic and B. Radovcic, "Electroweak breaking and Dark Matter from the common scale," Phys. Lett. B **732** (2014) 91–94, `arXiv:1401.8183 [hep-ph]`.

[50] V. V. Khoze, C. McCabe, and G. Ro, "Higgs vacuum stability from the dark matter portal," JHEP **08** (2014) 026, `arXiv:1403.4953 [hep-ph]`.

[51] S. Benic and B. Radovcic, "Majorana dark matter in a classically scale invariant model," JHEP **01** (2015) 143, `arXiv:1409.5776 [hep-ph]`.

[52] H. Okada and Y. Orikasa, "Classically conformal radiative neutrino model with gauged B − L symmetry," Phys. Lett. B **760** (2016) 558–564, `arXiv:1412.3616 [hep-ph]`.

[53] J. Guo, Z. Kang, P. Ko, and Y. Orikasa, "Accidental dark matter: Case in the scale invariant local B-L model," Phys. Rev. **D91** no.~11, (2015) 115017, `arXiv:1502.00508 [hep-ph]`.

[54] P. Humbert, M. Lindner, and J. Smirnov, “The Inverse Seesaw in Conformal Electro-Weak Symmetry Breaking and Phenomenological Consequences,” JHEP **06** (2015) 035, arXiv:1503.03066 [hep-ph].

[55] S. Oda, N. Okada, and D.-s. Takahashi, “Classically conformal U(1)’ extended standard model and Higgs vacuum stability,” Phys. Rev. D **92** no.~1, (2015) 015026, arXiv:1504.06291 [hep-ph].

[56] P. Humbert, M. Lindner, S. Patra, and J. Smirnov, “Lepton Number Violation within the Conformal Inverse Seesaw,” JHEP **09** (2015) 064, arXiv:1505.07453 [hep-ph].

[57] A. D. Plascencia, “Classical scale invariance in the inert doublet model,” JHEP **09** (2015) 026, arXiv:1507.04996 [hep-ph].

[58] N. Haba, H. Ishida, N. Okada, and Y. Yamaguchi, “Bosonic seesaw mechanism in a classically conformal extension of the Standard Model,” Phys. Lett. B **754** (2016) 349–352, arXiv:1508.06828 [hep-ph].

[59] A. Das, N. Okada, and N. Papapietro, “Electroweak vacuum stability in classically conformal B-L extension of the Standard Model,” Eur. Phys. J. C **77** no.~2, (2017) 122, arXiv:1509.01466 [hep-ph].

[60] N. Haba, H. Ishida, R. Takahashi, and Y. Yamaguchi, “Gauge coupling unification in a classically scale invariant model,” JHEP **02** (2016) 058, arXiv:1511.02107 [hep-ph].

[61] Z.-W. Wang, F. S. Sage, T. G. Steele, and R. B. Mann, “Asymptotic Safety in the Conformal Hidden Sector?,” J. Phys. G **45** no.~9, (2018) 095002, arXiv:1511.02531 [hep-ph].

[62] A. Das, S. Oda, N. Okada, and D.-s. Takahashi, “Classically conformal U(1)’ extended standard model, electroweak vacuum stability, and LHC Run-2 bounds,” Phys. Rev. D **93** no.~11, (2016) 115038, arXiv:1605.01157 [hep-ph].

[63] S. Oda, N. Okada, and D.-s. Takahashi, “Right-handed neutrino dark matter in the classically conformal U(1)’ extended standard model,” Phys. Rev. D **96** no.~9, (2017) 095032, arXiv:1704.05023 [hep-ph].

[64] T. Hambye, A. Strumia, and D. Teresi, “Super-cool Dark Matter,” JHEP **08** (2018) 188, arXiv:1805.01473 [hep-ph].

[65] F. Loebbert, J. Miczajka, and J. Plefka, “Consistent Conformal Extensions of the Standard Model,” Phys. Rev. D **99** no.~1, (2019) 015026, arXiv:1805.09727 [hep-ph].

[66] S. Yaser Ayazi and A. Mohamadnejad, “Conformal vector dark matter and strongly first-order electroweak phase transition,” JHEP **03** (2019) 181, arXiv:1901.04168 [hep-ph].

[67] Y. G. Kim, K. Y. Lee, and S.-H. Nam, “Conformal invariance and singlet fermionic dark matter,” Phys. Rev. D **100** no.~7, (2019) 075038, arXiv:1906.03390 [hep-ph].

[68] I. D. Gialamas, A. Karam, T. D. Pappas, and V. C. Spanos, “Scale-invariant quadratic gravity and inflation in the Palatini formalism,” Phys. Rev. D **104** no.~2, (2021) 023521, arXiv:2104.04550 [astro-ph.CO].

[69] B. Barman and A. Ghoshal, “Scale invariant FIMP miracle,” JCAP **03** no.~03, (2022) 003, arXiv:2109.03259 [hep-ph].

[70] B. Barman and A. Ghoshal, “Probing pre-BBN era with Scale Invariant FIMP,” arXiv:2203.13269.

[71] C. D. Carone and R. Ramos, "Classical scale-invariance, the electroweak scale and vector dark matter," Phys. Rev. **D88** (2013) 055020, arXiv:1307.8428 [hep-ph].

[72] G. M. Pelaggi, "Predictions of a model of weak scale from dynamical breaking of scale invariance," Nucl. Phys. B **893** (2015) 443–458, arXiv:1406.4104 [hep-ph].

[73] A. Karam and K. Tamvakis, "Dark matter and neutrino masses from a scale-invariant multi-Higgs portal," Phys. Rev. **D92** no.~7, (2015) 075010, arXiv:1508.03031 [hep-ph].

[74] V. V. Khoze and A. D. Plascencia, "Dark Matter and Leptogenesis Linked by Classical Scale Invariance," JHEP **11** (2016) 025, arXiv:1605.06834 [hep-ph].

[75] L. Chataignier, T. Prokopec, M. G. Schmidt, and B. Świeżewska, "Single-scale Renormalisation Group Improvement of Multi-scale Effective Potentials," JHEP **03** (2018) 014, arXiv:1801.05258 [hep-ph].

[76] D. Marfatia and P.-Y. Tseng, "Gravitational wave signals of dark matter freeze-out," JHEP **02** (2021) 022, arXiv:2006.07313 [hep-ph].

[77] K. A. Meissner and H. Nicolai, "Conformal Symmetry and the Standard Model," Phys. Lett. **B648** (2007) 312–317, arXiv:hep-th/0612165 [hep-th].

[78] R. Foot, A. Kobakhidze, and R. R. Volkas, "Electroweak Higgs as a pseudo-Goldstone boson of broken scale invariance," Phys. Lett. **B655** (2007) 156–161, arXiv:0704.1165 [hep-ph].

[79] R. Foot, A. Kobakhidze, K. McDonald, and R. Volkas, "Neutrino mass in radiatively-broken scale-invariant models," Phys. Rev. **D76** (2007) 075014, arXiv:0706.1829 [hep-ph].

[80] R. Foot, A. Kobakhidze, K. L. McDonald, and R. R. Volkas, "A Solution to the hierarchy problem from an almost decoupled hidden sector within a classically scale invariant theory," Phys. Rev. **D77** (2008) 035006, arXiv:0709.2750 [hep-ph].

[81] R. Foot, A. Kobakhidze, and R. R. Volkas, "Stable mass hierarchies and dark matter from hidden sectors in the scale-invariant standard model," Phys. Rev. D **82** (2010) 035005, arXiv:1006.0131 [hep-ph].

[82] L. Alexander-Nunneley and A. Pilaftsis, "The Minimal Scale Invariant Extension of the Standard Model," JHEP **09** (2010) 021, arXiv:1006.5916 [hep-ph].

[83] R. Foot, A. Kobakhidze, and R. R. Volkas, "Cosmological constant in scale-invariant theories," Phys. Rev. D **84** (2011) 075010, arXiv:1012.4848 [hep-ph].

[84] J. S. Lee and A. Pilaftsis, "Radiative Corrections to Scalar Masses and Mixing in a Scale Invariant Two Higgs Doublet Model," Phys. Rev. **D86** (2012) 035004, arXiv:1201.4891 [hep-ph].

[85] A. Farzinnia, H.-J. He, and J. Ren, "Natural Electroweak Symmetry Breaking from Scale Invariant Higgs Mechanism," Phys. Lett. **B727** (2013) 141–150, arXiv:1308.0295 [hep-ph].

[86] E. Gabrielli, M. Heikinheimo, K. Kannike, A. Racioppi, M. Raidal, and C. Spethmann, "Towards Completing the Standard Model: Vacuum Stability, EWSB and Dark Matter," Phys. Rev. **D89** no.~1, (2014) 015017, arXiv:1309.6632 [hep-ph].

[87] T. G. Steele, Z.-W. Wang, D. Contreras, and R. B. Mann, "Viable dark matter via radiative symmetry breaking in a scalar singlet Higgs portal extension of the standard model," Phys. Rev. Lett. **112** no.~17, (2014) 171602, arXiv:1310.1960 [hep-ph].

[88] J. Guo and Z. Kang, "Higgs Naturalness and Dark Matter Stability by Scale Invariance," Nucl. Phys. **B898** (2015) 415–430, arXiv:1401.5609 [hep-ph].

[89] A. Salvio and A. Strumia, "Agravity," JHEP **06** (2014) 080, arXiv:1403.4226 [hep-ph].

[90] H. Davoudiasl and I. M. Lewis, "Right-Handed Neutrinos as the Origin of the Electroweak Scale," Phys. Rev. **D90** no.~3, (2014) 033003, arXiv:1404.6260 [hep-ph].

[91] A. Farzinnia and J. Ren, "Higgs Partner Searches and Dark Matter Phenomenology in a Classically Scale Invariant Higgs Boson Sector," Phys. Rev. D **90** no.~1, (2014) 015019, arXiv:1405.0498 [hep-ph].

[92] M. Lindner, S. Schmidt, and J. Smirnov, "Neutrino Masses and Conformal Electro-Weak Symmetry Breaking," JHEP **10** (2014) 177, arXiv:1405.6204 [hep-ph].

[93] Z. Kang, "Upgrading sterile neutrino dark matter to FI*m*P using scale invariance," Eur. Phys. J. C **75** no.~10, (2015) 471, arXiv:1411.2773 [hep-ph].

[94] K. Kannike, G. Hütsi, L. Pizza, A. Racioppi, M. Raidal, A. Salvio, and A. Strumia, "Dynamically Induced Planck Scale and Inflation," JHEP **05** (2015) 065, arXiv:1502.01334 [astro-ph.CO].

[95] K. Endo and Y. Sumino, "A Scale-invariant Higgs Sector and Structure of the Vacuum," JHEP **05** (2015) 030, arXiv:1503.02819 [hep-ph].

[96] Z. Kang, "View FImP miracle (by scale invariance) à la self-interaction," Phys. Lett. B **751** (2015) 201–204, arXiv:1505.06554 [hep-ph].

[97] K. Endo and K. Ishiwata, "Direct detection of singlet dark matter in classically scale-invariant standard model," Phys. Lett. B **749** (2015) 583–588, arXiv:1507.01739 [hep-ph].

[98] A. Ahriche, K. L. McDonald, and S. Nasri, "A Radiative Model for the Weak Scale and Neutrino Mass via Dark Matter," JHEP **02** (2016) 038, arXiv:1508.02607 [hep-ph].

[99] Z.-W. Wang, T. G. Steele, T. Hanif, and R. B. Mann, "Conformal Complex Singlet Extension of the Standard Model: Scenario for Dark Matter and a Second Higgs Boson," JHEP **08** (2016) 065, arXiv:1510.04321 [hep-ph].

[100] K. Ghorbani and H. Ghorbani, "Scalar Dark Matter in Scale Invariant Standard Model," JHEP **04** (2016) 024, arXiv:1511.08432 [hep-ph].

[101] A. Farzinnia and S. Kouwn, "Classically scale invariant inflation, supermassive WIMPs, and adimensional gravity," Phys. Rev. D **93** no.~6, (2016) 063528, arXiv:1512.05890 [hep-ph].

[102] A. J. Helmboldt, P. Humbert, M. Lindner, and J. Smirnov, "Minimal conformal extensions of the Higgs sector," JHEP **07** (2017) 113, arXiv:1603.03603 [hep-ph].

[103] A. Ahriche, K. L. McDonald, and S. Nasri, "The Scale-Invariant Scotogenic Model," JHEP **06** (2016) 182, arXiv:1604.05569 [hep-ph].

[104] A. Ahriche, A. Manning, K. L. McDonald, and S. Nasri, "Scale-Invariant Models with One-Loop Neutrino Mass and Dark Matter Candidates," Phys. Rev. D **94** no.~5, (2016) 053005, arXiv:1604.05995 [hep-ph].

[105] F. Wu, "Aspects of a nonminimal conformal extension of the standard model," Phys. Rev. D **94** no.~5, (2016) 055011, arXiv:1606.08112 [hep-ph].

[106] S. Yaser Ayazi and A. Mohamadnejad, "Scale-Invariant Two Component Dark Matter," Eur. Phys. J. C **79** no.~2, (2019) 140, arXiv:1808.08706 [hep-ph].

[107] I. Oda, "Planck and Electroweak Scales Emerging from Conformal Gravity," Eur. Phys. J. C **78** no.~10, (2018) 798, arXiv:1806.03420 [hep-th].

[108] V. Brdar, Y. Emonds, A. J. Helmboldt, and M. Lindner, "Conformal Realization of the Neutrino Option," Phys. Rev. D **99** no.~5, (2019) 055014, arXiv:1807.11490 [hep-ph].

[109] V. Brdar, A. J. Helmboldt, and J. Kubo, "Gravitational Waves from First-Order Phase Transitions: LIGO as a Window to Unexplored Seesaw Scales," JCAP **02** (2019) 021, arXiv:1810.12306 [hep-ph].

[110] A. Mohamadnejad, "Accidental scale-invariant Majorana dark matter in leptoquark-Higgs portals," Nucl. Phys. B **949** (2019) 114793, arXiv:1904.03857 [hep-ph].

[111] K. Kannike, A. Kubarski, and L. Marzola, "Geometry of Flat Directions in Scale-Invariant Potentials," Phys. Rev. D **99** no.~11, (2019) 115034, arXiv:1904.07867 [hep-ph].

[112] D.-W. Jung, J. Lee, and S.-H. Nam, "Scalar dark matter in the conformally invariant extension of the standard model," Phys. Lett. B **797** (2019) 134823, arXiv:1904.10209 [hep-ph].

[113] V. Brdar, A. J. Helmboldt, and M. Lindner, "Strong Supercooling as a Consequence of Renormalization Group Consistency," JHEP **12** (2019) 158, arXiv:1910.13460 [hep-ph].

[114] J. Braathen, S. Kanemura, and M. Shimoda, "Two-loop analysis of classically scale-invariant models with extended Higgs sectors," JHEP **03** (2021) 297, arXiv:2011.07580 [hep-ph].

[115] K. Kannike, K. Loos, and L. Marzola, "Minima of classically scale-invariant potentials," JHEP **06** (2021) 128, arXiv:2011.12304 [hep-ph].

[116] J. Kubo, J. Kuntz, M. Lindner, J. Rezacek, P. Saake, and A. Trautner, "Unified emergence of energy scales and cosmic inflation," JHEP **08** (2021) 016, arXiv:2012.09706 [hep-ph].

[117] A. Ahriche, "Purely Radiative Higgs Mass in Scale invariant models," Nucl. Phys. B **982** (2022) 115896, arXiv:2110.10301 [hep-ph].

[118] R. Soualah and A. Ahriche, "Scale invariant scotogenic model: Dark matter and the scalar sector," Phys. Rev. D **105** no.~5, (2022) 055017, arXiv:2111.01121 [hep-ph].

[119] A. G. Dias, C. A. de S. Pires, V. Pleitez, and P. S. Rodrigues da Silva, "Dynamically induced spontaneous symmetry breaking in 3-3-1 models," Phys. Lett. B **621** (2005) 151–159, arXiv:hep-ph/0503192.

[120] M. Holthausen, M. Lindner, and M. A. Schmidt, "Radiative Symmetry Breaking of the Minimal Left-Right Symmetric Model," Phys. Rev. D **82** (2010) 055002, arXiv:0911.0710 [hep-ph].

[121] M. Heikinheimo, A. Racioppi, M. Raidal, C. Spethmann, and K. Tuominen, "Physical Naturalness and Dynamical Breaking of Classical Scale Invariance," Mod. Phys. Lett. **A29** (2014) 1450077, arXiv:1304.7006 [hep-ph].

[122] D. Chway, T. H. Jung, H. D. Kim, and R. Dermisek, "Radiative Electroweak Symmetry Breaking Model Perturbative All the Way to the Planck Scale," Phys. Rev. Lett. **113** no.~5, (2014) 051801, arXiv:1308.0891 [hep-ph].

[123] M. Holthausen, J. Kubo, K. S. Lim, and M. Lindner, "Electroweak and Conformal Symmetry Breaking by a Strongly Coupled Hidden Sector," JHEP **12** (2013) 076, arXiv:1310.4423 [hep-ph].

[124] J. Kubo, K. S. Lim, and M. Lindner, "Gamma-ray Line from Nambu-Goldstone Dark Matter in a Scale Invariant Extension of the Standard Model," JHEP **09** (2014) 016, arXiv:1405.1052 [hep-ph].

[125] W. Altmannshofer, W. A. Bardeen, M. Bauer, M. Carena, and J. D. Lykken, "Light Dark Matter, Naturalness, and the Radiative Origin of the Electroweak Scale," JHEP **01** (2015) 032, arXiv:1408.3429 [hep-ph].

[126] O. Antipin, M. Redi, and A. Strumia, "Dynamical generation of the weak and Dark Matter scales from strong interactions," JHEP **01** (2015) 157, arXiv:1410.1817 [hep-ph].

[127] G. F. Giudice, G. Isidori, A. Salvio, and A. Strumia, "Softened Gravity and the Extension of the Standard Model up to Infinite Energy," JHEP **02** (2015) 137, arXiv:1412.2769 [hep-ph].

[128] Y. Ametani, M. Aoki, H. Goto, and J. Kubo, "Nambu-Goldstone Dark Matter in a Scale Invariant Bright Hidden Sector," Phys. Rev. D **91** no.~11, (2015) 115007, arXiv:1505.00128 [hep-ph].

[129] C. D. Carone and R. Ramos, "Dark chiral symmetry breaking and the origin of the electroweak scale," Phys. Lett. B **746** (2015) 424–429, arXiv:1505.04448 [hep-ph].

[130] J. Kubo and M. Yamada, "Scale and electroweak first-order phase transitions," PTEP **2015** no.~9, (2015) 093B01, arXiv:1506.06460 [hep-ph].

[131] A. Latosinski, A. Lewandowski, K. A. Meissner, and H. Nicolai, "Conformal Standard Model with an extended scalar sector," JHEP **10** (2015) 170, arXiv:1507.01755 [hep-ph].

[132] N. Haba, H. Ishida, N. Kitazawa, and Y. Yamaguchi, "A new dynamics of electroweak symmetry breaking with classically scale invariance," Phys. Lett. B **755** (2016) 439–443, arXiv:1512.05061 [hep-ph].

[133] A. Karam and K. Tamvakis, "Dark Matter from a Classically Scale-Invariant $SU(3)_X$," Phys. Rev. **D94** no.~5, (2016) 055004, arXiv:1607.01001 [hep-ph].

[134] J. Kubo and M. Yamada, "Scale genesis and gravitational wave in a classically scale invariant extension of the standard model," JCAP **1612** no.~12, (2016) 001, arXiv:1610.02241 [hep-ph].

[135] H. Ishida, S. Matsuzaki, and R. Ouyang, "Unified interpretation of scalegenesis in conformally extended standard models: a dynamical origin of Higgs portal," Chin. Phys. C **44** no.~11, (2020) 111002, arXiv:1907.09176 [hep-ph].

[136] A. G. Dias, J. Leite, B. L. Sánchez-Vega, and W. C. Vieira, "Dynamical symmetry breaking and fermion mass hierarchy in the scale-invariant 3-3-1 model," Phys. Rev. D **102** no.~1, (2020) 015021, arXiv:2005.00556 [hep-ph].

[137] M. Aoki, V. Brdar, and J. Kubo, "Heavy dark matter, neutrino masses, and Higgs naturalness from a strongly interacting hidden sector," Phys. Rev. D **102** no.~3, (2020) 035026, arXiv:2007.04367 [hep-ph].

[138] A. G. Dias, J. Leite, and B. L. Sánchez-Vega, "Scale-invariant 3-3-1-1 model with $B-L$ symmetry," arXiv:2207.06276 [hep-ph].

[139] C. Gross, O. Lebedev, and Y. Mambrini, "Non-Abelian gauge fields as dark matter," JHEP **08** (2015) 158, arXiv:1505.07480 [hep-ph].

[140] T. Hambye, "Hidden vector dark matter," JHEP **01** (2009) 028, arXiv:0811.0172 [hep-ph].

[141] D. Croon, O. Gould, P. Schicho, T. V. I. Tenkanen, and G. White, "Theoretical uncertainties for cosmological first-order phase transitions," JHEP **04** (2021) 055, arXiv:2009.10080 [hep-ph].

[142] P. Athron, C. Balazs, A. Fowlie, L. Morris, G. White, and Y. Zhang, "How arbitrary are perturbative calculations of the electroweak phase transition?," arXiv:2208.01319 [hep-ph].

[143] J. Ellis, M. Lewicki, and J. M. No, "On the Maximal Strength of a First-Order Electroweak Phase Transition and its Gravitational Wave Signal," JCAP **04** (2019) 003, arXiv:1809.08242 [hep-ph].

[144] J. Ellis, M. Lewicki, J. M. No, and V. Vaskonen, "Gravitational wave energy budget in strongly supercooled phase transitions," JCAP **06** (2019) 024, arXiv:1903.09642 [hep-ph].

[145] M. Lewicki and V. Vaskonen, "On bubble collisions in strongly supercooled phase transitions," Phys. Dark Univ. **30** (2020) 100672, arXiv:1912.00997 [astro-ph.CO].

[146] J. Ellis, M. Lewicki, and J. M. No, "Gravitational waves from first-order cosmological phase transitions: lifetime of the sound wave source," JCAP **07** (2020) 050, arXiv:2003.07360 [hep-ph].

[147] J. Ellis, M. Lewicki, and V. Vaskonen, "Updated predictions for gravitational waves produced in a strongly supercooled phase transition," JCAP **11** (2020) 020, arXiv:2007.15586 [astro-ph.CO].

[148] V. K. Shante and S. Kirkpatrick, "An introduction to percolation theory," Advances in Physics **20** no.~85, (1971) 325–357. https://doi.org/10.1080/00018737100101261.

[149] **XENON** Collaboration, E. Aprile et al., "Dark Matter Search Results from a One Ton-Year Exposure of XENON1T," Phys. Rev. Lett. **121** no.~11, (2018) 111302, arXiv:1805.12562 [astro-ph.CO].

[150] **PandaX-4T** Collaboration, Y. Meng et al., "Dark Matter Search Results from the PandaX-4T Commissioning Run," Phys. Rev. Lett. **127** no.~26, (2021) 261802, arXiv:2107.13438 [hep-ex].

[151] **LZ** Collaboration, J. Aalbers et al., "First Dark Matter Search Results from the LUX-ZEPLIN (LZ) Experiment," arXiv:2207.03764 [hep-ex].

[152] **XENON** Collaboration, E. Aprile et al., "Projected WIMP sensitivity of the XENONnT dark matter experiment," JCAP **11** (2020) 031, arXiv:2007.08796 [physics.ins-det].

[153] M. T. Frandsen, M. E. Thing, M. Heikinheimo, K. Tuominen, and M. Rosenlyst, "Vector dark matter in supercooled Higgs portal models," arXiv:2301.00041 [hep-ph].

[154] C. Caprini, M. Chala, G. C. Dorsch, M. Hindmarsh, S. J. Huber, T. Konstandin, J. Kozaczuk, G. Nardini, J. M. No, K. Rummukainen, P. Schwaller, G. Servant, A. Tranberg, and D. J. Weir, "Detecting gravitational waves from cosmological phase transitions with LISA: an update," Journal of Cosmology and Astroparticle Physics **2020** no.~03, (Mar, 2020) 024–024. https://doi.org/10.1088

[155] T. Robson, N. J. Cornish, and C. Liu, "The construction and use of LISA sensitivity curves," Classical and Quantum Gravity **36** no.~10, (Apr, 2019) 105011. https://doi.org/10.1088%2F1361-6382%2Fab1101.